Syngas Chemical Looping Gasification Process: Bench-Scale Studies and Reactor Simulations

Fanxing Li, Liang Zeng, Luis G. Velazquez-Vargas, Zachary Yoscovits, and Liang-Shih Fan
William G. Lowrie Dept. of Chemical and Biomolecular Engineering,
The Ohio State University, Columbus, OH 43210

DOI 10.1002/aic.12093
Published online December 14, 2009 in Wiley InterScience (www.interscience.wiley.com).

The syngas chemical looping process co-produces hydrogen and electricity from syngas through the cyclic reduction and regeneration of an iron oxide based oxygen carrier. In this article, the reducer, which reduces the oxygen carrier with syngas, is investigated through thermodynamic analysis, experiments, and ASPEN Plus® simulation. The thermodynamic analysis indicates that the countercurrent moving-bed reducer offers better gas and solids conversions when compared to the fluidized-bed reducer. The reducer is continuously operated for 15 h in a bench scale moving-bed reactor. A syngas conversion in excess of 99.5% and an oxygen carrier conversion of nearly 50% are obtained. An ASPEN Plus® model is developed which simulates the reducer performance. The results of simulation are consistent with those obtained from both the thermodynamic analysis and experiments. Both the experiments and simulation indicate that the proposed SCL reducer concept is feasible. © 2009 American Institute of Chemical Engineers *AIChE J,* 56: 2186–2199, 2010

Keywords: chemical looping, gasification, coal, hydrogen, electricity, moving bed

Introduction

Hydrogen is an important feedstock for oil refining and ammonia synthesis. It is also an environmentally friendly energy carrier. The demand for hydrogen has been increasing at a rate of 4% each year and such a trend is expected to continue.[1] To meet the ever increasing demand for affordable hydrogen, an efficient hydrogen production technique from an abundant energy source needs to be developed. At present, about 50% of the hydrogen is produced from natural gas reforming processes. The volatile natural gas prices in recent years have led to serious consideration of hydrogen production using coal. Coal can be converted to hydrogen through the well established coal gasification – water gas shift (WGS) processes.[2] However, due to the elaborate syngas cleaning and conditioning and gas separation requirements, such a process is capital intensive and relatively inefficient when compared to the natural gas reforming process, especially under a CO_2 constrained environment. With the pressing needs for clean, efficient and cost/energy effective coal-to-hydrogen processes, the chemical looping technique has evolved as an important alternative to the traditional techniques.

The chemical looping process that generates end products with the aid of chemical intermediates through a series of reaction schemes was first applied for industrial practice between the late 19th century and the early 20th century. Howard Lane[3] from England was among the first researchers/engineers who conceived and successfully commercialized the steam-iron process for hydrogen production using the chemical looping principle. Using the iron oxide chemical intermediate, the steam-iron process generates H_2 from reducing gas obtained from coal and steam through an indirect reaction scheme.[3,4] Although the adoption of the chemical looping strategy in the early years was mainly prompted by the lack of effective chemical conversion/separation techniques in the product generation, modern applications of chemical looping processes are prompted by the need of developing an optimized reaction scheme that minimizes the exergy loss involved in the chemical/energy conversion

Correspondence concerning this article should be addressed to L.-S. Fan at fan@chbmeng.ohio-state.edu.

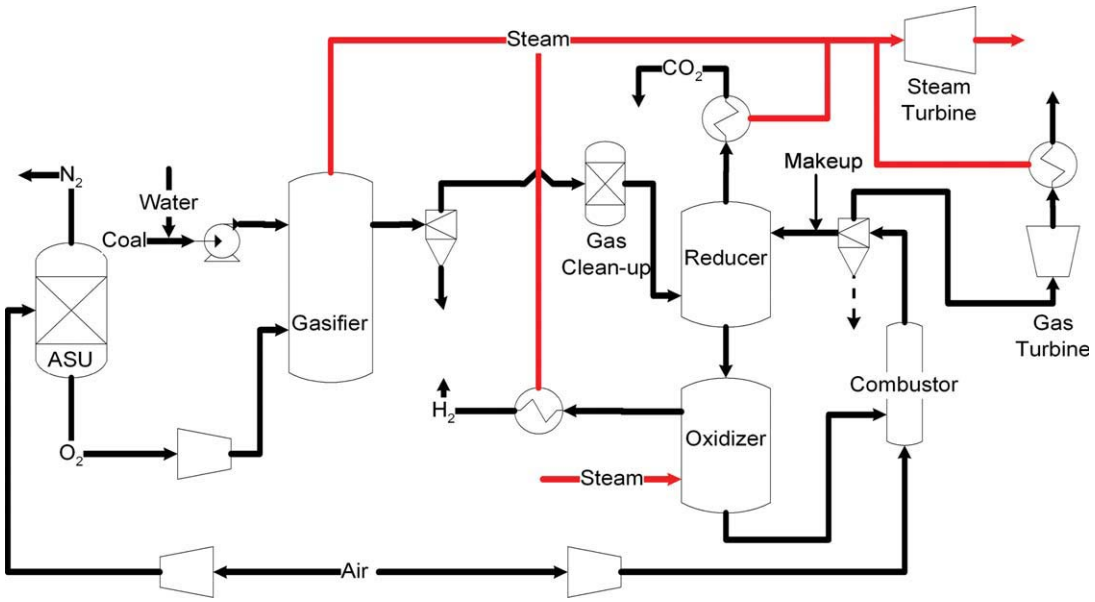

Figure 1. Simplified schematic of the syngas chemical looping process.

[Color figure can be viewed in the online issue, which is available at www.interscience.wiley.com.]

system.[5–7] Also driven by the envisaged CO_2 emission control, the recent development in chemical looping systems has focused on the efficient conversion of gaseous carbonaceous fuels such as natural gas and coal derived syngas,[7–11] and solid fuels such as petroleum coke and coal[12,13] although separating CO_2 readily through the looping reaction scheme.

The chemical looping processes can generally be described based on *chemical looping combustion (CLC)* and *chemical looping gasification*. In the chemical looping combustion, metal oxide is first reduced with fuels and the reduced metal oxide is then combusted with air to generate heat for electricity production.[14] In the chemical looping gasification, metal oxide is first reduced with fuels and the reduced metal oxide is then reacted with steam and/or carbon dioxide to form hydrogen and/or carbon monoxide. The hydrogen and/or carbon monoxide can then be used to produce liquid fuels, chemicals and electricity.[15] Chemical looping combustion systems are being conducted extensively at various scales.[9,16–20] Recent research on chemical looping gasification processes, however, is mostly limited to conceptual studies. Svodoba et al.[21,22] examined, using thermodynamic principles, the feasibility of using Fe, Mn, Ni, Cr, and Co based particles for hydrogen production. They concluded that Fe–Fe_3O_4 is more suitable for chemical looping gasification compared to other particles; they stated that Fe_3O_4 is difficult to be reduced using a fluidized bed. Xiang et al. performed ASPEN Plus® simulation of an iron-based looping system for hydrogen generation.[23] In their system, reduced iron oxide is only regenerated to Fe_3O_4 rather than Fe_2O_3. As a result, a significant amount of syngas will leave the reducer unconverted. Therefore, a chemical looping gasification scheme that effectively converts both iron oxide and the gaseous fuel is desired for efficient hydrogen and power generation.

In this article, the syngas chemical looping (SCL) gasification process[10,24–28] is described. The process converts gaseous fuels such as coal derived syngas into hydrogen and electricity through the aid of an iron based oxygen carrier particle, avoiding the water gas shift and CO_2 separation steps. Specifically, the syngas chemical looping process is first described. A thermodynamic analysis is then performed, reflecting a desired countercurrent moving-bed reducer design. It is followed by experimental results obtained from a bench scale moving-bed reactor. Finally, a multistage ASPEN Plus® model is developed to simulate the reducer performance. The simulation results show a good consistency with both the thermodynamic analysis and the experimental results. The feasibility of the syngas chemical looping concept is validated with both the bench scale testing and simulations.

Syngas Chemical Looping (SCL) Process Overview and Thermodynamic Analysis of the Reactors

SCL process overview

Figure 1 shows the schematic flow diagram of the syngas chemical looping process. In the SCL process, raw syngas is produced from a conventional coal gasifier. The particulates in the raw syngas are then removed using high-temperature filters such as a candle filter. This is followed by a hot-gas cleaning step at 400°C for bulk sulfur removal. The particulate free-raw syngas after the hot-gas cleaning has H_2S at the level of ppm range; it is then introduced to a reducer operated at 750–900 °C and 30 atm. The reducer is a countercurrent moving-bed reactor with Fe_2O_3 fed from the top and syngas introduced from the bottom. The main reactions in the reducer include

$$Fe_2O_3 + CO/H_2 \rightarrow 2FeO + CO_2/H_2O$$

$$FeO + CO/H_2 \rightarrow Fe + CO_2/H_2O$$

The impurities in the syngas stream such as sulfur compounds and elemental mercury after the hot-gas cleaning

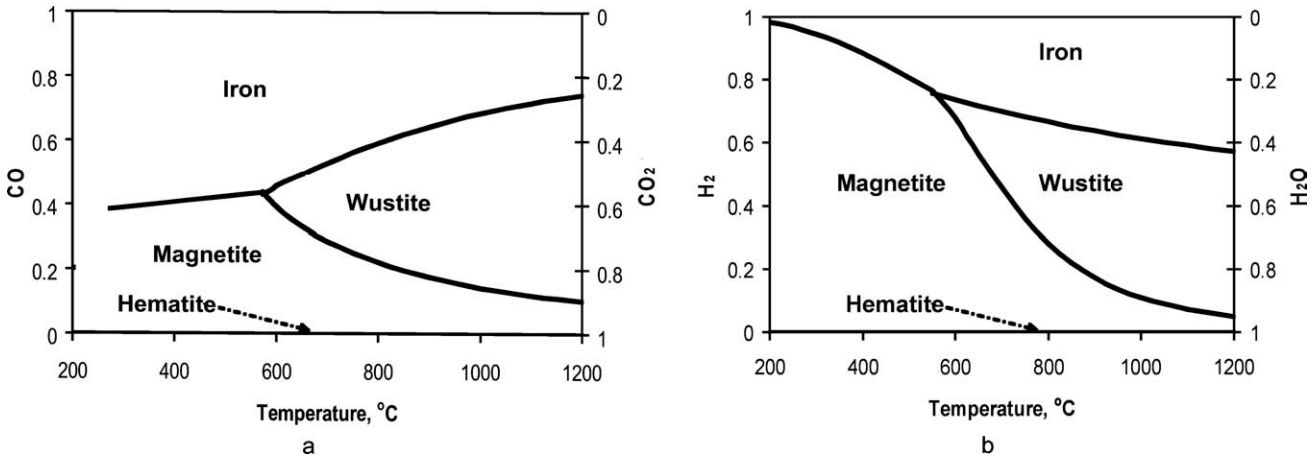

Figure 2. Equilibrium phase diagrams of (a) iron-carbon-oxygen system, and (b) iron-hydrogen-oxygen system.

will not react with the iron oxide. Therefore, these pollutants will leave the reducer along with the CO_2 and steam resulted from syngas oxidation. After pollutant removal and steam condensation, the concentrated CO_2 stream can be further compressed and sequestrated.

The iron oxides exiting from the bottom of the reducer are mainly in the form of FeO and Fe. Such a solid stream is then introduced to the oxidizer operated using a countercurrent moving bed at 500–800°C and 30 atm. The oxidizer converts steam into hydrogen although regenerating FeO and Fe to Fe_3O_4. The main reactions in the oxidizer are

$$3Fe + 4H_2O \rightarrow Fe_3O_4 + 4H_2$$

$$3FeO + H_2O \rightarrow Fe_3O_4 + H_2$$

The gaseous product from the oxidizer is a mixture of hydrogen and steam. Steam is condensed out to obtain a concentrated hydrogen stream.

Fe_3O_4 formed in the reducer is regenerated to Fe_2O_3 in a combustor. The combustor is a riser that conveys particles to the reducer by pressurized air. The combustor also serves as a heat generator since a significant amount of heat is produced during combustion of Fe_3O_4 to Fe_2O_3

$$4Fe_3O_4 + O_2 \rightarrow 6Fe_2O_3$$

The high-pressure, high-temperature gas produced from the combustor can be used for electricity generation to compensate the parasitic energy consumptions. In yet another configuration, part or all of the reduced particles from the reducer can be directly sent to the combustor without reacting with steam in the oxidizer. By doing so, more heat will be available for the electricity generation whereas the hydrogen generation will decrease. As can be seen, in this looping process, hydrogen is generated from the oxidizer whereas CO_2 and other contaminants are generated from the reducer. Therefore, the energy required for CO_2 separation, product purification, and contaminant removal is reduced.

Thermodynamic Analysis of Reducer and Selection of Gas-Solid Flow Pattern

Unlike the oxidation reaction in the combustor which is intrinsically fast and is thermodynamically favored, the reactions in the reducer and the oxidizer are limited by the thermodynamic equilibriums and are relatively slow. An optimal reducer and oxidizer design that maximizes the solid and gas conversions via a thermodynamically favored gas-solid contact scheme, is, therefore, desirable. As described in the previous section, the reducer and oxidizer in the SCL process employ countercurrent moving-bed reactors. A simple thermodynamic analysis of the reducer is performed to illustrate the choice of using countercurrent moving bed. The performance of both a fluidized-bed reducer and a countercurrent moving-bed reducer is analyzed.

The goal of the thermodynamic analysis is to determine the maximum gas and solid conversions of a fluidized-bed reducer and a moving-bed reducer. It is noted that the thermodynamic analysis predicts the gas and solid conversions under the thermodynamic equilibrium. Such equilibrium can only be reached under the condition of the reaction being sufficiently fast and/or the gas-solid contact time in the reactor being sufficiently long. The reactions conducted in the chemical looping processes are under this condition, and, therefore, it is expected that the thermodynamic analysis can estimate the performance of the looping reactors with reasonable accuracy.[2,29]

Figure 2 shows the equilibrium gas compositions of the iron-carbon-oxygen system and the iron-hydrogen-oxygen system at different temperatures.[30,31] It is noted that FeO is used here to represent wustite, whose exact formula varies with the temperature. From the phase diagrams, the equilibrium gas concentrations for different oxidation states of iron may vary significantly at any given temperatures. The high concentrations of CO and/or hydrogen equilibrate with iron at lower oxidation states, whereas the high CO_2 and/or steam concentrations co-exist with the higher oxidations states of iron.

For illustration purposes, pure H_2 and pure Fe_2O_3 are used as the gas and solid reactants for the reducer operated at

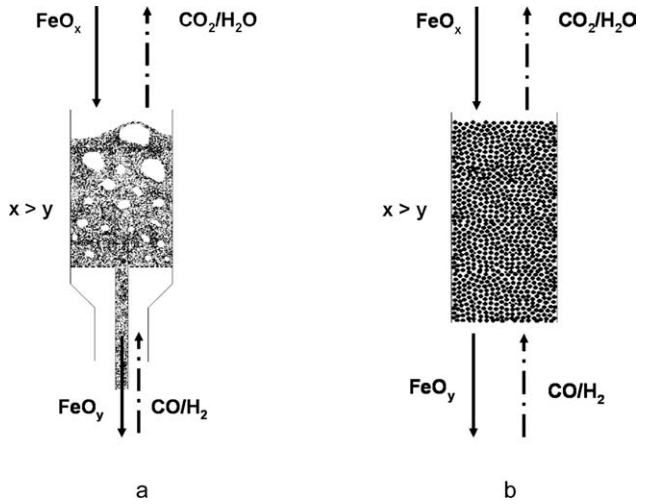

Figure 3. Gas-solid contact pattern of the reducer using (a) fluidized-bed design, and (b) moving-bed design.

850°C. The ratio between the solid and gas molar flow rate is set to be s. The conversions of H_2 and Fe_2O_3 are denoted as x and y, respectively. The Fe_2O_3 conversion y is defined as

$$y = \frac{n_O/n_{Fe} - \hat{n}_O/\hat{n}_{Fe}}{n_O/n_{Fe}} \times 100\% \tag{1}$$

Here n_O/n_{Fe} is the molar ratio of oxygen atom to iron atom in Fe_2O_3, and $\hat{n}_O/\hat{n}_{Fe}$ is the molar ratio of oxygen atom to iron atom in the converted solid product, i.e., FeO_x ($0 < x < 1.5$). The support material is treated as an inert. Therefore, the oxygen atoms associated with the inert ingredient are not included in Eq. 1.

When H_2 is the only reducing gas, the reactions in the reducer include

$$H_2 + 3Fe_2O_3 \leftrightarrows H_2O + 2Fe_3O_4$$
$$K_1 = P_{H_2O}/P_{H_2} = 1.92 \times 10^4 \ @850\ ^\circ C$$
$$H_2 + Fe_3O_4 \leftrightarrows H_2O + 3FeO$$
$$K_2 = P_{H_2O}/P_{H_2} = 3.5454 \ @850\ ^\circ C$$
$$H_2 + FeO \leftrightarrows H_2O + Fe$$
$$K_3 = P_{H_2O}/P_{H_2} = 0.5344 \ @850\ ^\circ C$$

K_1–K_3 are the equilibrium constants which can be readily obtained from Figure 2b.

Fluidized-bed reducer

In a fluidized-bed reactor such as a dense-phase fluidized bed, significant mixing for the gas and the solid in the reactor occurs. Thus, in a fluidized-bed reducer (Figure 3a), the fresh syngas reactant will be diluted by the gaseous product which is rich in H_2O and CO_2. From Figure 3, the dilution by CO_2 and H_2O decreases the reducing capability of the syngas. Similarly, the mixing of solids in a fluidized bed results in a discharge of the low-conversion solids from the fluidized bed. Therefore, the gas and solid conversions in the fluidized-bed reducer are limited. A similar constraint applies when a fluidized-bed reactor is used as the oxidizer.

To illustrate the effect of mixing, it is assumed that both the solid and the gas are well mixed in a fluidized-bed reactor in the following analysis. The oxygen mass balance on the reactor can be given as

$$x = 3sy \tag{2}$$

This equation indicates that the oxygen depleted from the solid is transferred to the gas through the formation of steam or CO_2. Meanwhile, the thermodynamic equilibrium gives

$$K_n = x/(1-x) \tag{3}$$

Here, n is 1, 2, or 3 depending on the phase of iron in the reducer. According to Figure 2, when excessive Fe_2O_3 is present ($0 \le y < 11.11\%$), the equilibrium constant will follow K_1; when Fe_3O_4 and FeO mixture is present ($11.11\% \le y < 33.33\%$), the equilibrium gas composition is determined by K_2; when FeO and Fe are co-existing ($33.33\% \le y < 100\%$), the equilibrium constant will follow K_3.

Equations 2 and 3 can be solved together to arrive at the relationship between the gas and the solid conversions (x, y), and the ratio of the solid to gas-flow rates. It can be shown that x is a step function with respect to s as

$$x = \begin{cases} K_1/(K_1+1) & s > 3K_1/(K_1+1) \\ s/3 & 3K_1/(K_1+1) \ge s > 3K_2/(K_2+1) \\ K_2/(K_2+1) & 3K_2/(K_2+1) \ge s > K_2/(K_2+1) \\ s & K_2/(K_2+1) \ge s > K_3/(K_3+1) \\ K_3/(K_3+1) & K_3/(K_3+1) \ge s > K_3/(K_3+1) \\ 3s & s \le K_3/3(K_3+1) \end{cases} \tag{4}$$

y can be obtained from x using Eq. 2

$$y = x/3s \tag{5}$$

For a fluidized-bed reducer operated at 850°C, the solid and gas conversions can be obtained by substituting the values of K_1–K_3 to Eqs. 4 and 5

$$x = \begin{cases} 1 & s > 3.0 \\ s/3 & 3.0 \ge s > 2.34 \\ 0.78 & 2.34 \ge s > 0.78 \\ s & 0.78 \ge s > 0.348 \\ 0.348 & 0.348 \ge s > 0.116 \\ 3s & s \le 0.116 \end{cases} \tag{6}$$

$$y = \begin{cases} 0.3333/s & s > 3.0 \\ 0.1111 & 3.0 \ge s > 2.34 \\ 0.26/s & 2.34 \ge s > 0.78 \\ 0.3333 & 0.78 \ge s > 0.348 \\ 0.116/s & 0.348 \ge s > 0.116 \\ 1 & s \le 0.116 \end{cases} \tag{7}$$

Figure 4a shows the relationship between the gas and the solid conversions and the ratio between the solid and the gas-molar flow rates. Figure 4a′ shows the relationship

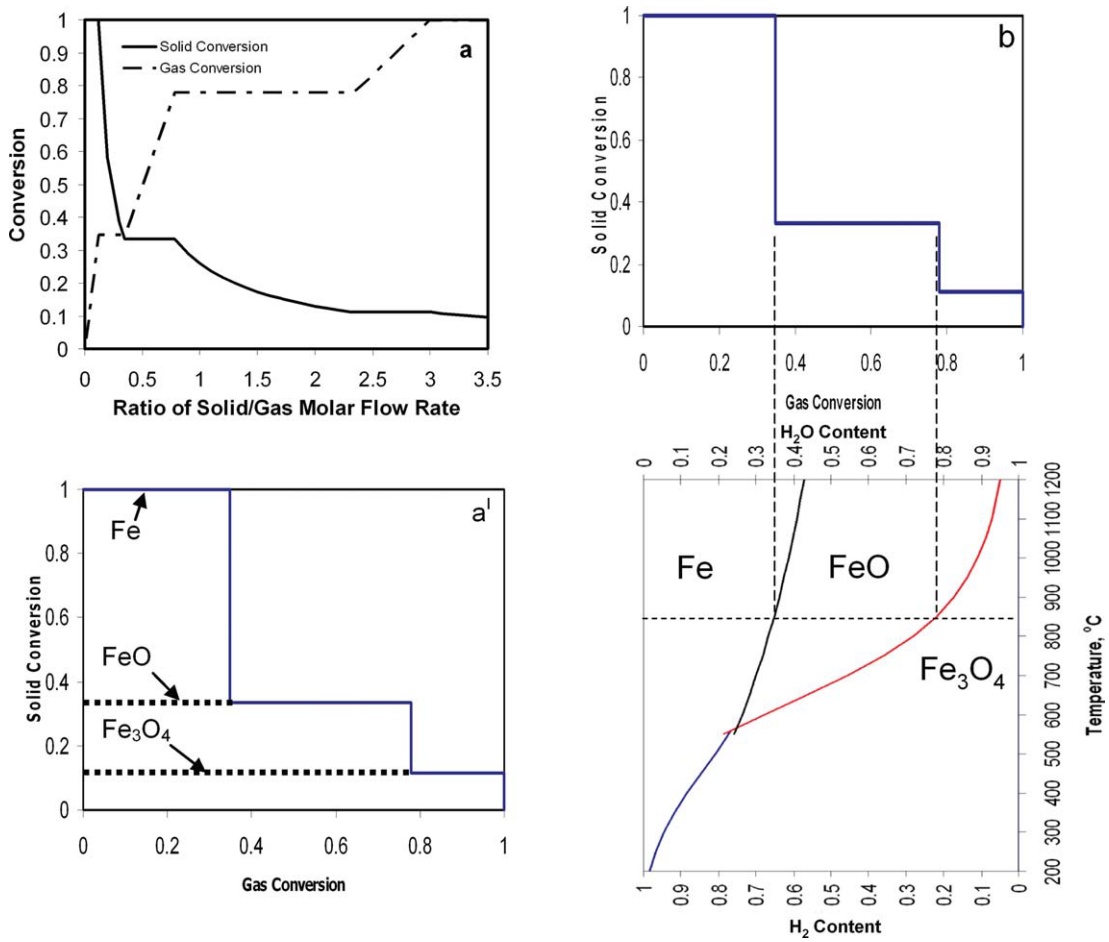

Figure 4. Operating curves for a fluidized-bed reactor (a) solid and gas conversion vs. solid/gas molar flow rate ratio derived from analytical approach, (a′) relationship between the solid conversion and gas conversion derived from analytical approach, and (b) derivation of operating curve from thermodynamic phase diagram.

[Color figure can be viewed in the online issue, which is available at www.interscience.wiley.com.]

between the gas and the solid conversions. Since, for a fluidized-bed reducer, the gas and solid conversions at any steady state operating conditions will fall on the curves shown in Figure 4a and Figure 4a′, these curves are noted as the operating curves.[28] As can be seen, the conversions of gas and solid are inversely correlated, i.e., a higher-solid conversion corresponds to a lower-gas conversion and vice versa. In the actual reactor operation, a full conversion of fuel is crucial. Figure 4a′ shows a gas conversion of 100% corresponding to a solid conversion of less than 11.11%.

The operating curve for the fluidized bed can also be derived directly from the thermodynamic phase diagram. The rationale being that since the solid and gas are well mixed and are at the thermodynamic equilibrium, the gas and solid concentrations should be at the equilibrium concentrations described by the thermodynamic phase diagram. Thus, the operating curve should coincide with the gas-solid equilibrium curve. The translation of the equilibrium phase diagram into the fluidized-bed operating curve is illustrated in Figure 4b. The vertical dashed line describes the relationship between the phases of iron and the equilibrium gas concentration at a certain temperature (850°C as in the figure). For a fluidized-bed reducer, the equilibrium steam concentration is identical to the hydrogen conversion x in the operating curve. The phases of iron that equilibrate with such a gas concentration determine the solid conversion y defined by Eq. 1. For instance, a solid conversion of 100% corresponds to pure iron, whereas a solid conversion of 33.33% corresponds to pure FeO. It is noted that the operating curve under the equilibrium condition divides the graph into two regions. Since the gas and the solid conversions will always be lower than or equal to those at equilibrium in practical reactor operations, the gas and solid conversions will approach the equilibrium line from its lefthand side as the gas and solid contact time increases. The thermodynamics dictates that these conversions will not cross the equilibrium line.

Countercurrent moving-bed reactor

Contrary to the fluidized-bed reactor, a moving-bed reactor has the minimal axial mixing of either gas or solids. When a moving bed reactor with a countercurrent gas-solid contact pattern is used as the reducer (Figure 3b), a fresh syngas feed with high H_2 and CO concentrations will react

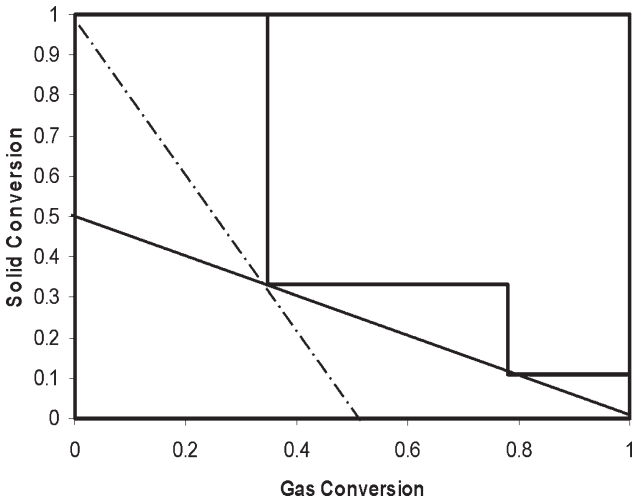

Figure 5. Operating lines in a countercurrent moving-bed reactor under 850°C.

Solid line: operating line with full syngas conversion and maximum solid conversion, dotted line: operating line with full solid conversion and maximum gas conversion.

with iron at lower-oxidation states. Meanwhile, the partially converted syngas with low H_2 and CO concentrations will react with iron at higher-oxidation states. Based on the thermodynamic diagram shown in Figure 4, such a contact pattern will maximize both the solid and gas conversions. A similar case can also be expected when a moving-bed reactor is used as the oxidizer. With the mixing for both the solid and the gas phases negligible in the moving bed reactor, both the gas and solid compositions will vary with the axial position of the moving-bed reactor. The mass balance of oxygen in an infinitesimal layer between z and $z + \Delta z$ of the moving-bed reactor at a steady state can be written as

$$3s(y_{z+\Delta z} - y_z) = (x_z - x_{z+\Delta z}) \tag{8}$$

Equation 8 can be expressed by

$$dx/dy = -3s \tag{9}$$

Thus, the relationship between the solid conversion $\boldsymbol{y}$, and the gas conversion $\boldsymbol{x}$, under a certain solid/gas molar flow rate ratio $\boldsymbol{s}$, is a straight line with a slope of $-3\boldsymbol{s}$. Such a line represents the operating line. The operating line is only restricted by thermodynamic equilibrium. Specifically, at any point of the operating line, the ratio of the concentration between steam and hydrogen should not be higher than the equilibrium constant K

$$\begin{aligned} x/(1-x) &\le \mathrm{K}_1 \quad \text{for} \quad 0 \le y < 0.1111 \\ x/(1-x) &\le \mathrm{K}_2 \quad \text{for} \quad 0.1111 \le y < 0.3333 \\ x/(1-x) &\le \mathrm{K}_3 \quad \text{for} \quad 0.3333 \le y < 1 \end{aligned} \tag{10}$$

These equations can be expressed by

$$\begin{aligned} x &\le \mathrm{K}_1/(1+\mathrm{K}_1) \quad \text{for} \quad 0 \le y < 0.1111 \\ x &\le \mathrm{K}_2/(1+\mathrm{K}_2) \quad \text{for} \quad 0.1111 \le y < 0.3333 \\ x &\le \mathrm{K}_3/(1+\mathrm{K}_3) \quad \text{for} \quad 0.3333 \le y < 1 \end{aligned} \tag{11}$$

The aforementioned restrictions are in conformity with the earlier discussion, which indicates that a practical reducer operating line should locate at the lefthand side of the equilibrium line and should not cross it. Thus, the feasible operating lines can be determined based on the mass balance and thermodynamic phase diagram. Two possible operating lines are shown in Figure 5.

It can be shown that each point on the operating line corresponds to the gas/solid conversions on a certain axial position of the moving-bed reactor. The theoretical gas and solid conversions can be obtained from the intercept of the operating line with the x and y axes. The intercept of the operating line with the y axis corresponds to the solid conversion at the solid outlet located at the bottom of the reactor where the highest possible solid conversion is achieved. Similarly, the intercept of the operating line with x axis is the gas conversion at the gas outlet located at the top of the reactor. For example, the solid line in Figure 5 corresponds to a solid/gas molar flow ratio of 1:1.5. Under this operating condition, H_2 will be 100% converted and the solid will be reduced by ~50%. Since the operating line is restricted to the lefthand side of the equilibrium curve, it is not possible to achieve 100% conversions simultaneously for the gas and the solid. In fact, the solid line corresponds to the maximum achievable solid conversion when H_2 is fully converted. Similarly, to achieve a full solid conversion, at least 92% excessive H_2 over the stoichiometric requirement needs to be introduced to the reactor, yielding a maximum gas conversion of ~52%.

With Figure 5, the optimum gas and solid flow rates for the SCL reducer can be determined. For example, a full conversion of syngas is essential for the reducer since incomplete syngas gas conversion will lead to a reduced energy conversion efficiency. Therefore, the optimum operating line is the solid line in Figure 5, which corresponds to a solid conversion of ~50%. It can also be shown that multiple-stage interconnected fluidized-bed reactors with countercurrent gas and solid contact pattern can achieve a conversion similar to that of the moving bed. In contrast, a single-stage fluidized-bed reducer can achieve merely an 11.11% solid conversion under the same operating conditions. When utilized as an oxidizer, a moving bed is also anticipated to achieve higher conversions. Since improved gas and solid conversions enhance the overall efficiency of the chemical looping gasification scheme, a countercurrent moving bed is used as the reducer or the oxidizer. Results from both experiments and ASPEN Plus® simulation in the following sections further illustrate the performance of a moving-bed reducer.

Experimental Methods

Reactor setup

A bench-scale moving-bed reactor with a maximum capacity of 2.5 kW_{th} (kilo-watts thermal) is used to test the SCL reactor operations.[32] The moving-bed reactor is a scale up of the one that is described by Gupta et al.[32] The reactor

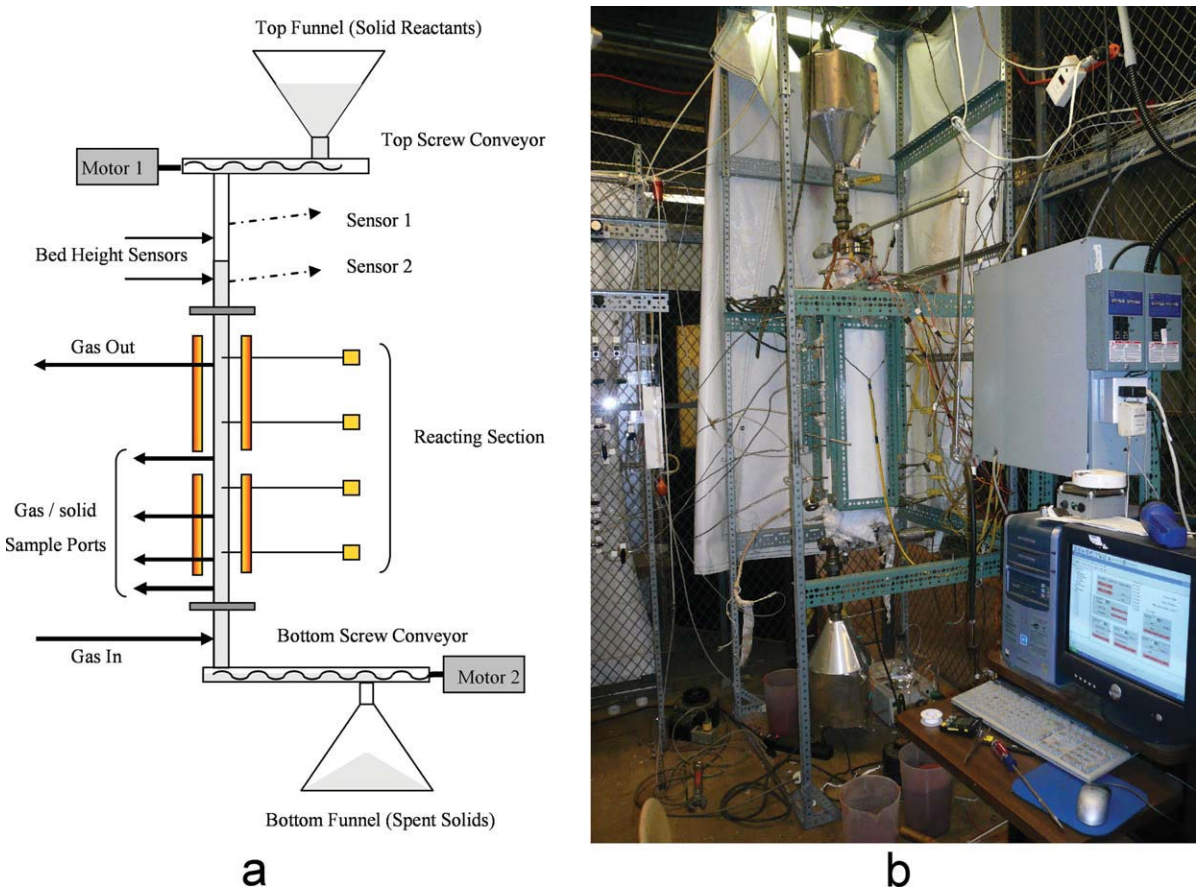

Figure 6. Bench-scale demonstration unit for SCL process (a) schematic flow diagram of the unit, and (b) photograph of the unit.

[Color figure can be viewed in the online issue, which is available at www.interscience.wiley.com.]

setup is illustrated in Figure 6. The reactor can be operated at the solid-flow rates up to 82 g/min (4.9 kg/h), and the gas-flow rates up to 200 mL/s (12 L/min). The heated reaction section of the reactor has an I.D. (inner dia.) of 1.6 in. (4.06 cm), and a bed height of 40 in. (101.6 cm). In a typical experiment, solid reactants such as oxygen carrier particle are first loaded to the top funnel; the screw conveyor system then transports the solids steadily from the top funnel to the bottom funnel through the moving-bed reactor. The solid level in the moving-bed reactor is maintained at a constant level by a bed height detecting system. Reactant gases are introduced from the gas inlet located at the bottom of the moving bed and react with the solids in a countercurrent manner. The gas composition along the axial positions of the reactor is constantly monitored using a Varian CP-4900 micro GC. The solid samples are taken from the solid sampling ports after the experiments for characterization. The moving bed setup directly mimics the gas-solid contact pattern of the reducer and oxidizer in the syngas chemical looping process.

Experimental procedure

The goal of the experiments is to demonstrate the continuous operation of the reducer at ambient pressure. Before the experiments, 14 kg of composite pellets with 60% Fe_2O_3 (by weight) and 40% inert support is loaded to the top funnel. The solid-flow rate is then adjusted by changing the speed of the screw conveyors followed by solid-flow rate calibration. The solid-flow rate in this experiment is 12.87 g/min. After solid flow rate calibration, the reactor is sealed and flushed overnight using N_2 at a flow rate of 500 mL/min. Prior to heating up the reactor, gas samples from various sections of the reactor are analyzed using a Varian CP-4900 MicroGC to confirm that the oxygen content in the reactor is low. The pressurized helium leak test is also conducted to examine potential gas leakage. After the oxygen test and leak test, the solid-transport system is activated to continuously feed the particles to the reactor. Meanwhile, the reactor is gradually heated up to ~900°C. Once a steady solid flow in the reactor is achieved, simulated syngas that consists of CO, H_2, and CO_2 is introduced into the bottom of the reactor. The composition of the simulated syngas is similar to that from a Shell gasifier. In this experiment, N_2 is also introduced along with the simulated syngas. The flow rates of the gas mixture used in the experiments are shown in Table 1.

After the reactant gas is introduced, the gas compositions at the various positions of the reactor are constantly monitored and sampled using the MicroGC. The steady state with respect to the gas and solid conversions along the reactor usually takes one solid residence time to establish. In the

Table 1. Gas-Flow Rates to the Bench-Scale Unit

Gas Type	N_2	CO	H_2	CO_2
Flow Rate (ml/min)	498.1	990.0	660.3	113.6
Composition (mol %)	22.02	43.77	29.19	5.02

experiments, the steady state condition is maintained for more than 13 h. During the experiments, a slight increase in the flow rates of syngas beyond that given in Table 1 is attempted; however, a notable increase in the CO and H_2 concentrations are observed at the reactor outlet. The observation implies that the solid-flow rates of 12.87 g/min cannot sustain a full conversion of the syngas when its flow rates are higher than those given in Table 1.

At the end of the experiments, the flows of the reactant gas and the solid and the reactor heating elements are simultaneously switched off. The reactor is flushed with N_2 until it is cooled down to the room temperature. The solid samples at various positions along the reactor are taken from the solid sampling ports. Each of these samples is then divided into two portions. One portion is characterized using a CM-120 total carbon analyzer (UIC, Inc.) for carbon content. The remaining is oxidized in a PerkinElmer Pyris 1 Thermal-Gravimetric Analyzer using air. The solid conversions are determined based on the weight change measured in the TGA, and the carbon content measured by the carbon analyzer.

The solid-particle conversion $\boldsymbol{y}$ defined in Eq. 1 can be calculated through the following equation

$$y = \frac{W_1 - W_0(1 - c\%)}{0.3 \times W_1 \times L\%} \times 100\% \tag{12}$$

Here W_0 is the weight of the converted sample before oxidized by air (in TGA). W_1 is the weight of the sample after air oxidation. c is the percentage of carbon in the converted sample obtained from the carbon analyzer. L is the percentage of iron oxide in the composite pellets.

Simulation Model and Methods

Although the operating lines, as given in Figures 4 and 5, obtained from thermodynamic analysis are useful, they are rather difficult to be constructed and applied. One alternative method is to use computer simulation method based on the Advanced System for Process Engineering software, or ASPEN Plus®. The comprehensive physical and thermodynamic property data banks built in the ASPEN Plus® software render it suitable for reactor steady-state simulation.

Table 2. Parameters for the ASPEN Plus® Model

Name of the Parameter	Parameter Setting
Reactor Module	RGIBBS
Physical and Thermodynamic Databanks	COMBUST, INORGANIC, SOLIDS and PURE
Stream Class	MIXCISLD
Chemical Components	Listed in Table 5
Property Method (for Gas and Liquid)	PR-BM*
Calculation Algorism	Sequential Modular (SM)

*Property methods for solids are discussed separately, and some correlative parameters are presented in Table 4.

Selection of ASPEN Plus® modeling parameters

The RGIBBS module is used to determine the equilibrium conditions. The key parameters such as physical and thermodynamic property data banks and property methods, stream classes, chemical components, and calculation algorithms are listed in Tables 2 to 4. It is noted that modifications to the physical property data and physical property methods for the solids are often necessary in order to obtain consistent results from the literature and from the ASPEN Plus® simulation.

The INORGANIC databank in the ASPEN Plus® software, which determines the physical and thermodynamic properties of the solids at various conditions, uses Barin equation (Eq. 9) and its CPSXP (a-h) coefficients[33] to obtain the Gibbs energy (G), enthalpy (H), entropy (S), and heat capacity (C_p) for the solids

$$\begin{aligned} G &= a + bT + cT\ln T + dT^2 + eT^3 + fT^4 + gT^{-1} + hT^{-2} \\ H &= a - cT - dT^2 - 2eT^3 - 3fT^4 + 2gT^{-1} + 3hT^{-2} \\ S &= -b - c(1 + \ln T) - 2dT - 3eT^2 - 4fT^3 + gT^{-2} + 2hT^{-3} \\ C_p &= -c - 2dT - 6dT^2 - 12fT^3 - 2gT^{-2} - 6hT^{-3} \end{aligned} \tag{13}$$

Table 4 lists the CPSXP coefficients for iron and its oxides in the INORGANIC databank in ASPEN Plus®. The HSC® chemistry 5.1, and other literature sources were used to verify the values of these coefficients.[34–37] In doing so, the reference states in the literature sources were adjusted to be identical to that specified in ASPEN Plus®, i.e., 25°C and 1 atm. Minor differences were found in coefficients a, b, and c for Fe_3O_4 and FeO ($Fe_{0.947}O$). The differences amount to ~1% of the original values in the ASPEN databank. Although the differences are rather small, the simulation

Table 3. Components List in Reducer Simulation£

Component ID	Stream Type	Component name	Formula
CO	CONV	CARBON-MONOXIDE	CO
CO_2	CONV	CARBON-DIOXIDE	CO_2
H_2	CONV	HYDROGEN	H_2
H_2O	CONV	WATER	H_2O
Fe_2O_3	SOLID	HEMATITE	Fe_2O_3
Fe_3O_4	SOLID	MAGNETITE	Fe_3O_4
FeO	SOLID	WUESTITE	FeO
$Fe_{0.947}O$	SOLID	WUESTITE	$Fe_{0.947}O$
Fe	SOLID	IRON	Fe
C	SOLID	CARBON-GRAPHITE	C
Fe_3C	SOLID	TRIIRON-CARBIDE	Fe_3C
HG	CONV	MERCURY	Hg
HGS	CONV	MERCURY-SULFIDE-RED	HgS
S	CONV	SULFUR	S
H_2S	CONV	HYDROGEN-SULFIDE	H_2S
FeS	SOLID	IRON-MONOSULFIDE	FeS
$Fe_{0.877}S$	SOLID	PYRRHOTITE	$Fe_{0.877}S$

£Species such as FeS_2, HgO do not exist in the interested temperature range; therefore, they are not included.

Table 4. Parameters in the ORGANIC Databank in ASPEN Plus®

Components	FE_2O_3	FE_3O_4	FE	$FE_{0.947}O$
Temperature units	°C	°C	°C	°C
Property units	J/kmol	J/kmol	J/kmol	J/kmol
T1	25	576.8500000	25	25.00000000
T2	686.85	1596.850000	626.85	1376.850000
a	−9.28E+08	−9.7072850E+8	3.78E+07	−2.8212753E+8
a′	−9.28E+08	−9.5672850E+8	3.78E+07	−2.81844E+8
b	1.98E+06	5.27383876E+5	−6.54E+05	4.01635664E+5
b′	1.98E+06	5.355839E+05	−6.54E+05	4.029657E+05
c	−2.58E+05	−50171.18100	1.09E+05	−4.878544E+04
c′	1.98E+06	−5.089700E+04	−6.54E+05	−4.860400E+04
d	165.486384	−35.96733770	−214.129205	−4.184000020
e	−0.066806967	−6.0151695E-5	0.084705631	0.0
f	1.17E-05	6.12900216E-9	−1.95E-05	0.0
g	7.66E+09	−4.277784E+10	−4.01E+09	1.40164001E+8
h	−3.76E+11	5.46763727E+9	1.98E+11	0.0

The prime sign (′) denotes the revised values.

results can be significant varied, particularly with respect to the phase transition conditions of various iron states. It is determined, based on the various case studies presented in the following sections, that the revised values better represent the actual thermodynamic properties of iron oxides.

ASPEN Plus® model for fluidized-bed reactor

The equilibrium conditions in a fluidized-bed reactor are simulated using a simple RGIBBS module. With the modeling parameter selected, the fluidized-bed model can be set up by connecting reactants and products streams to the RGIBBS module and by inserting the operating conditions and inlet compositions into the ASPEN flow sheet.

Multistage ASPEN Plus® model for moving-bed reactor

A series of interconnected CSTR reactor based on RIGIBBS module is used to simulate the countercurrent moving-bed reactor. The model configuration is shown in Figure 7. As can be seen in the figure, the solid entering stage k is the solid product discharged from stage k + 1, whereas the gas entering stage k is the gaseous product of stage k − 1. It can be shown that such a model configuration satisfies the mass balance and thermodynamic restrictions imposed on a countercurrent moving-bed reactor. With a large number of RGIBBS blocks, the countercurrent moving-bed reactor can be approximated.

The simulation of a moving-bed system using an infinite number of RGIBBS blocks is not feasible. However, the simulation results show asymptotic behavior with increasing number of RGIBBS blocks. It is found, based on numerous case studies, that a five-stage model configuration can simulate the countercurrent moving bed with good accuracy. This is verified by comparing results obtained from a five-stage model with those obtained from a six-stage model. The comparisons indicate that the two models are identical in all cases. Therefore, the five-stage RGIBBS model is used to simulate the countercurrent moving-bed reactor.

Results and Discussion

Moving-bed experiments

Figure 8 shows the gas and solid conversions along the axial locations of the reactor at steady-state conditions. The carbon depositions along the reactor are given in Table 5, whereas the outlet gas compositions are given in Table 6. Further information regarding the performance of the oxygen carrier used in the SCL process is given in a preceding article.[38]

As can be seen in Table 5 and Figure 8, the solid is steadily converted as it moves toward the bottom of the reactor. The iron oxide conversion at the reactor outlet is 49.5%, which corresponds to a mixture of FeO (74.6%) and Fe (25.4%). Throughout the reactor, carbon deposition is not significant due to the relatively high-operating temperature and the presence of CO_2.[10] The carbon deposition can be further inhibited by increasing the CO_2 concentration in the syngas. The syngas conversion profile shows an opposite trend when

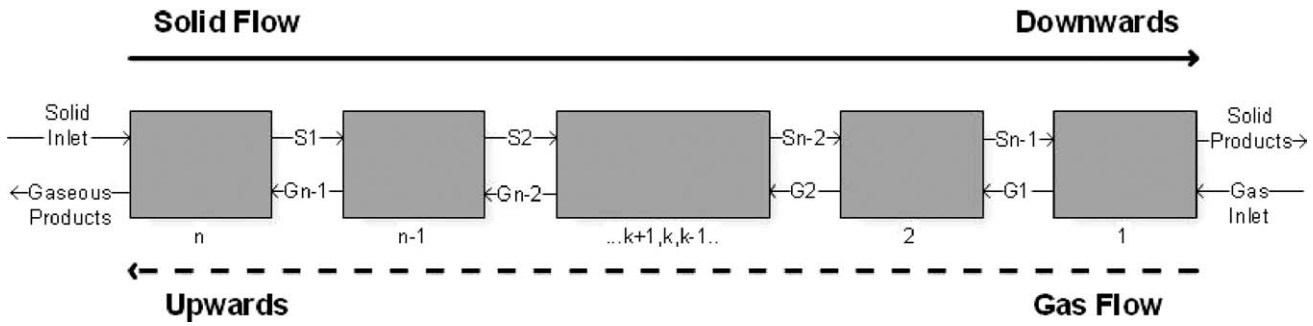

Figure 7. Arrangement of Multistage fluidized-bed system for the simulation of a moving bed.

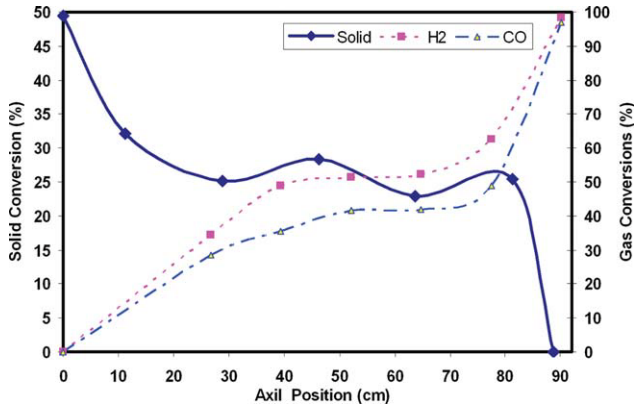

Figure 8. Experimental results for the gas and solid conversions in the reducer experiments (0 cm corresponds to gas inlet/solid outlet).

[Color figure can be viewed in the online issue, which is available at www.interscience.wiley.com.]

compared to the solid-conversion profile due to the countercurrent contact pattern between the solid and the gas. As can be seen in Table 6 and Figure 8, the syngas is near fully converted before exiting from the moving bed. The outlet gas is comprised mainly of CO_2 (dry, N_2 free basis). Another trend that can be observed from Figure 8 is that the gas and solid conversions are faster at the gas outlet/solid inlet when compared to the gas inlet/solid outlet. This is due to the faster reduction kinetics for the conversion of Fe_2O_3 to Fe_3O_4 when compared to the conversion of Fe_3O_4 to FeO and FeO to Fe. Moreover, little or no change in gas and solid conversions is observed in the middle part of the reactor. This is mainly due to the fact that the gas and solid compositions in this intermediate region are close to equilibrium. The results indicate that the solid-residence time can be shortened without affecting the reducer performance. The conversion profile of the gas is generally consistent to that of the solid. The minor fluctuation in the solid conversion along the axial locations of the reactor may result from the randomness of the solid sampling since the amount of the sample that can be extracted from the reactor is relatively small when compared to the size of the moving bed. The reducer simulation is performed as given in the following sections.

Comparisons between Thermodynamic Analysis and ASPEN Plus® Simulation

Fluidized-bed reducer simulation with hydrogen as the fuel

To obtain data comparable to those from the thermodynamic analysis, a sensitivity analysis is performed to determine the relationship between the gas and solid conversions in a fluidized bed by varying the mole flow rate ratio of Fe_2O_3 to H_2 (***s***). The operating temperature (850°C) for the simulation is identical to that in the thermodynamic analysis. The ASPEN simulation results are given in Figure 9. As can be seen from the figure, the simulation results are almost identical to those obtained from theoretical analysis given in Figure 4a.

Table 5. Solids Conversions and Carbon Depositions along the Reactor

Distance from the Reactor Bottom (cm)	88.75	81.25	63.75	46.25	28.75	11.25	0
Carbon percentage (wt %)	0	0.0283	0.0750	0.092	0.024	0.114	0.061
Solids conversion (%)	0	25.460	22.859	28.364	25.202	32.11	49.50

Table 6. Gas Composition at the Reactor Outlet Over Three Hours of Reactor Operation

Gas Type	CO	H_2	CO_2
Percentage (%)	0–0.41	0.001–0.1	99.5–99.999

Moving-bed reducer simulation with hydrogen as the fuel

The multistage Aspen Plus® model is used is to validate the (solid) operating line shown in Figure 5. The Fe_2O_3 to H_2 molar flow rate ratio ***s*** is set to be 1:1.5. The reactor is operated at 850°C. These conditions are identical to those denoted on the solid operating line in Figure 5, which shows a maximum solid conversion with near complete conversion of gas. The operating line derived from the multistage ASPEN Plus® model is plotted in Figure 10. As can be seen from Figures 5 and 10, the operating line shown derived from ASPEN Plus® simulation matches well to that derived from thermodynamic analysis. Table 7 compares the key results from the thermodynamic analysis to those from the ASPEN Plus® simulation. As can be seen, the results from the analysis and the simulation are consistent. This consistency confirms that the parameters in the modified thermodynamic data bank are accurate. Moreover, the multistage ASPEN Plus® model can simulate the performance of a countercurrent moving-bed reactor with good accuracy. The

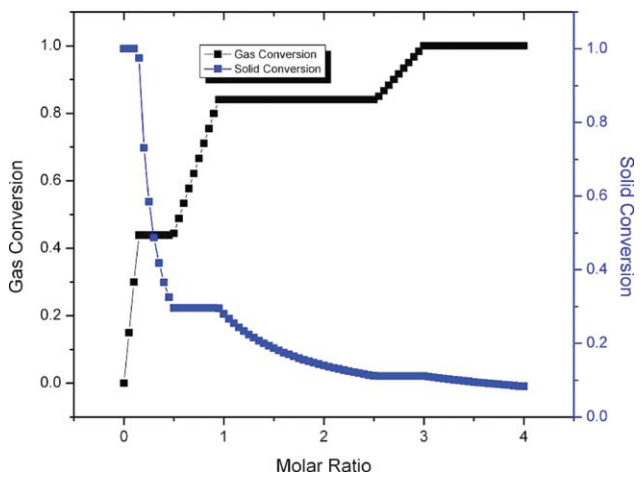

Figure 9. Simulation results for the operating curve of a fluidized-bed reducer at 850°C derived from ASPEN Plus®.

[Color figure can be viewed in the online issue, which is available at www.interscience.wiley.com.]

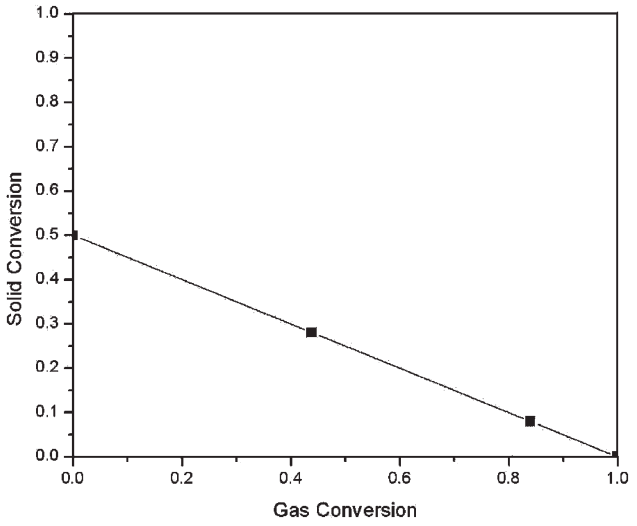

Figure 10. Simulation results for the operating line of a countercurrent moving-bed reducer derived from multistage model.

Operating conditions: temperature 850°C; pressure 1–30 atm; reducing gas H_2; Fe_2O_3 to H_2 molar flow rate ratio: 1:1.5.

multistage ASPEN Plus® model is further extended to simulate reducer at various operating conditions.

Comparisons between Experimental Results and ASPEN Plus® Simulation

The effect of varying the molar flow ratio of iron oxide to syngas gas (H_2: CO: CO_2: N_2 = 1:1.499:0.172:0.7544) in a reducer operated at 900°C is investigated using ASPEN Plus® simulation. Figure 10 shows the syngas and solid conversions under different iron oxide to syngas molar flow rate ratios. As can be seen from the figure, the iron oxide to syngas molar flow rate ratio should be no less than 1:1.41 in order to convert all the syngas. This corresponds to a maximum solid conversion of 46.9%. The case when the iron oxide to syngas molar flow rate ratio (***s***) is equal to 1:1.41 is simulated with the ASPEN Plus® multistage model. Table 8 is the material balance summary of the case, in which a syngas stream of 2.65 mol/h CO, 1.77 mol/h H_2, 1.33 mol/h N_2, and 0.304 mol/h CO_2 is introduced to a moving-bed reducer along with a countercurrent stream of 3.14 mol/h Fe_2O_3. The results suggest that almost all the reducing gas can be converted, whereas the solid is converted to wustite and metallic iron with a solid conversion of 46.9%. Table 9 further compares the gas and solid conversions obtained from the bench scale experiments with those achieved from the ASPEN® simulation.

As can be seen from Table 9, the ASPEN simulation results are reasonably consistent with the moving-bed experimental data. The slightly lower-solid conversion predicted by ASPEN Plus® simulation may result from either the inaccuracy of the CPSXP coefficients or the temperature distribution along the axial position of the moving-bed reactor, which ranges from 880–920 °C. It can be concluded from Table 9 that: (1) the multistage ASPEN Plus® simulation model can predict the thermodynamic performance of a moving-bed reactor with reasonable accuracy, and (2) the bench scale moving-bed reactor can achieve close to optimum gas and solid conversions predicted by the thermodynamic analysis. With the consistency between the thermodynamic analysis and the experimental results, the multistage ASPEN Plus® model developed in this study can assist the analysis and optimization of the SCL reactors.

Effects of Pressure, Temperature, and Pollutant Levels in Syngas

The utilization of the multistage ASPEN Plus® model for the SCL operating condition optimization and pollutant control strategy development is exemplified in this section. Effects of temperature, pressure, and pollutant levels in syngas on the reaction behavior are discussed.

Effect of pressure

Since the iron oxide reaction with CO and H_2 are isometric, the change in total pressure between 1 to 50 atm has little effect on the reaction equilibriums. No carbon deposition is predicted based on the ASPEN Plus® simulation. When other types of fuels such as methane or coal are used, the effect of pressure can be significant. This effect of pressure is well represented by the multistage model described earlier.

Effect of temperature

A higher-temperature favors the endothermic reaction, and a lower-temperature favors the exothermic reaction. The reaction between Fe_2O_3 and CO is exothermic whereas the reaction between Fe_2O_3 and H_2 is endothermic. Figure 12 shows the effect of temperature on the syngas conversion in a countercurrent moving-bed reactor. The reactor operating pressure is 30 atm with a stoichiometric amount of gaseous and solid reactants. The syngas is composed of 33% H_2 and 66% CO. This figure indicates that the equilibrium conversions of CO and H_2 show an opposite trend. A sharp increase in the syngas conversion is observed at ~580°C; beyond it the overall syngas conversion slowly decreases with the increase in temperature. The sharp increase in the syngas conversion at ~580°C is caused by the emergence of wustite phase, which does not exist below 550°C. Since the decrease in the overall syngas conversion is relatively slow

Table 7. Key Results from Thermodynamic Analysis and ASPEN Plus® Simulation of Countercurrent Moving-Bed Reducer Using Hydrogen as the Fuel

	Thermodynamic Analysis	ASPEN Plus® Simulation
Hydrogen Conversion when s = 1:1.5	99.995%	99.95%
Fe_2O_3 Conversion when s = 1:1.5	50.00%	49.98%
Hydrogen Conversion when s = 1:5.77	52%	52%
Fe_2O_3 Conversion when s = 1:5.77	100%	100%

Table 8. Molar Flow of Solid and Gas for the Moving-Bed Reducer Simulation

	Solid Flow Rates (mol/hr)				Gas Flow Rate (mol/hr)				
	Fe	$Fe_{0.947}O$	Fe_3O_4	Fe_2O_3	CO	CO_2	H_2	H_2O	N_2
Gas Inlet/Solid Outlet					2.65	0.304	1.77	0	1.33
Stage 1	1.54	5.00	0	0	1.80	1.15	0.96	0.81	1.33
Stage 2	0	6.53	0.03	0	0.51	2.44	0.24	1.53	1.33
Stage 3	0	0	1.51	0.88	0.002	2.95	0.001	1.77	1.33
Stage 4	0	0	0	3.14	0.002	2.95	0.001	1.77	1.33
Stage 5	0	0	0	3.14	0.002	2.95	0.001	1.77	1.33
Solid Inlet/Gas Outlet	0	0	0	3.14					

at temperatures above 600°C, the optimum operating temperature range for the reducer is determined to be 700 to 900°C due to the fast reaction kinetics at higher-temperatures.

Fates of sulfur and mercury

The pollutant control is essential for any coal conversion processes. H_2S, COS and mercury are important pollutants that present in coal derived syngas. The multistage model can assist in determining the fates of these pollutants. The ASPEN simulation is conducted to examine the relationship between the sulfur content in the syngas and the formation of iron-sulfur compounds. The potential compounds considered include S, COS, SO_2, H_2S, FeS, $Fe_{0.877}S$. At 900°C, 30 atm with ***s*** of 0.66 (1:1.5), the simulation results indicate that $Fe_{0.877}S$ is the only sulfur compound that may form in the reducer. As shown in Figure 13, no $Fe_{0.877}S$ will form particles unless the H_2S level in syngas is higher than 600 ppm. Similarly, unless the COS level exceeds 650 ppm, no sulfur will attach to the Fe_2O_3 particles. The practical implication of these simulation results is significant in that with the absence of sulfur attachment to the solids, the hydrogen product stream from the oxidizer will be sulfur free. Thus, the sulfur control strategy for the SCL process is simplified. Specifically, a hot-gas cleanup unit (HGCU) is installed at the upstream of the reducer for the bulk sulfur removal. Since the available high temperature sorbent can reduce the sulfur level in raw syngas to below 50 ppm with ease,[39] the remaining sulfur in the syngas will exit from the reducer along with CO_2 and H_2O. After condensing the steam, the sulfur containing CO_2 will be ready for geological sequestration.[40] Such a process arrangement avoids the energy intensive solvent based H_2S stripping process. Cooling and reheating of the syngas can also be avoided, rendering a more efficient sulfur control scheme.

Elemental mercury, the major form of mercury that presents in the raw syngas derived from coal, is commonly captured using activated carbon bed under a low-temperature in conventional coal gasification processes. From the ASPEN simulation, mercury will not react with any substances that are present in the reducer. Thus, all the mercury in the syngas stream will exit from the reducer flue gas and will not be present in the hydrogen stream from the oxidizer. The mercury containing flue gas from the oxidizer can be treated before sequestration using activated carbon. The mercury separation in this manner is more efficient than does the traditional process which involves the cooling and reheating of the syngas.

Table 9. Comparison of Experimental Outcomes and Simulation Results

	Experimental Results	ASPEN Plus® Simulations
Syngas Conversion (%)	99.5–99.999	99.898
Solids conversion (%)	49.5	46.9

Concluding Remarks

The performance of the reducer in the syngas chemical looping (SCL) process is investigated through thermodynamic analysis, experiments, and ASPEN Plus® simulation. The thermodynamic analysis indicates that a gas-solid countercurrent mode of operation in a moving bed reducer offers significantly better performance than does a gas-solid fluidized-bed reducer. Experiments on a bench scale moving-bed reactor indicate near complete conversion of syngas with close to 50% conversion of Fe_2O_3. The numerical simulation

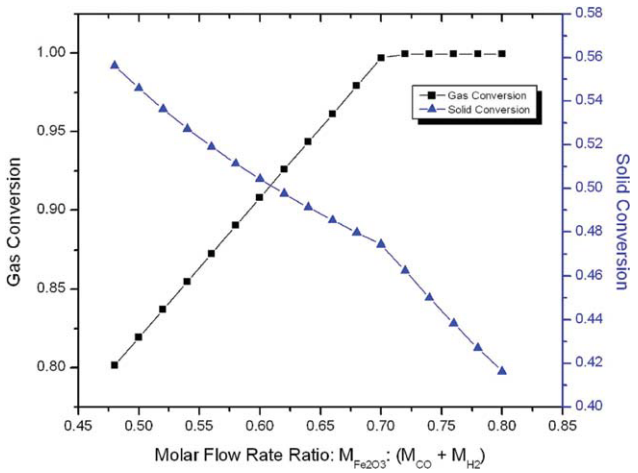

Figure 11. Simulation Results for the relationship between the gas and solid conversions, and solid to syngas gas molar flow rate ratio in a countercurrent moving bed.

Operating conditions: Temperature 900 °C; pressure 1 atm; syngas composition: CO 43.77%, H_2 29.19%, CO_2 5.02%, N_2 22.02%. [Color figure can be viewed in the online issue, which is available at www.interscience.wiley.com.]

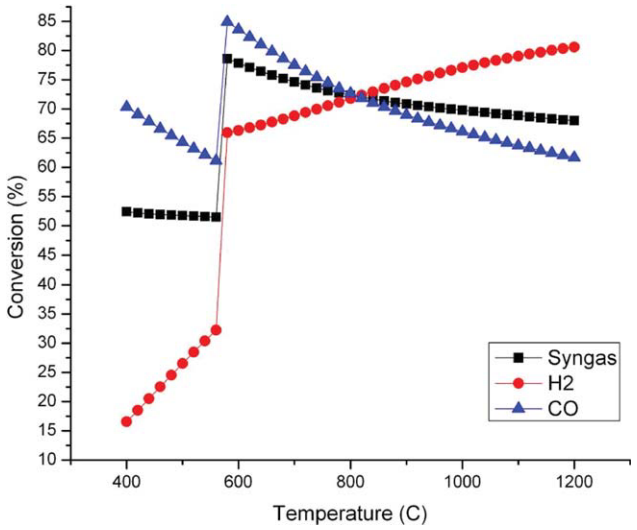

Figure 12. Simulation results for the effect of temperature on the conversions of syngas, CO, and H_2 in a countercurrent moving-bed reactor.

Operating conditions: pressure 30 atm; solid to gas molar flow rate ratio 0.33; syngas composition: H_2 33.3%, CO 66.6%. [Color figure can be viewed in the online issue, which is available at www.interscience.wiley.com.]

based on a multistage ASPEN Plus® model is developed for moving-bed simulation. The results of the ASPEN Plus® simulation corroborate those from thermodynamic analysis and experiments. The multistage ASPEN Plus® model, is, thus, shown effective in SCL reactor simulation and optimization. The model is also used to evaluate the SCL reducer performance under various operating conditions and for assisting the optimization of the pollutant control systems. Both the simulation and experimental results indicate that with a countercurrent moving bed operation, the gas and solid conversions in the reducer can reach a high level.

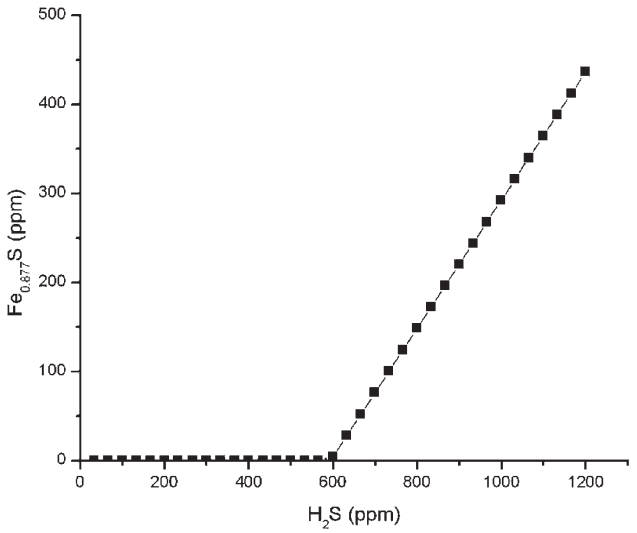

Figure 13. Simulation results for the relationship between the $Fe_{0.877}S$ formation and the syngas H_2S level in a countercurrent moving-bed reactor.

Operating conditions: Temperature 900°C; pressure 30 atm; solid to gas molar flow rate ratio 0.66.

Acknowledgments

This work was supported by the Ohio Coal Development Office of the Ohio Air Quality Development Authority (Project CDO/D-08-02), Ohio Dept. of Development (Project TECH 08-062), U. S. Dept. of Energy (Project DE-FC26-07NT43059), The Ohio State University and an industrial consortium.

Notation

s = molar flow rate ratio between the solid and the gas
x = hydrogen conversion
y = iron oxide conversion
n_o = moles of oxygen atom in a Fe_2O_3 sample before redox reactions
n_{Fe} = moles of iron atom in the same Fe_2O_3 sample before redox reactions
$\hat{n}_o$ = moles of oxygen atom in the same Fe_2O_3 sample after redox reactions
$\hat{n}_{Fe}$ = moles of iron atom in the same Fe_2O_3 sample after redox reactions
K = reaction equilibrium constant
x = normalized oxygen content of the reducer product
W_0 = weight of the oxygen carrier sample before oxidation with air
W_1 = weight of the oxygen carrier sample after oxidation with air
c = weight percentage of carbon in the oxygen carrier sample
L = weight percentage of iron oxide in the composite oxygen carrier pellets

Literature Cited

1. Udengaard NR. Hydrogen Production by Steam Reforming of Hydrocarbons. *Preprints of Symposia - American Chemical Society, Division of Fuel Chemistry*. 2004;49(2):906–907.
2. Higman C. *Gasification*. 2nd ed. Boston: Gulf Professional; 2008.
3. Lane H. Process for the Production of Hydrogen. US Patent 1078686. 1913.
4. Hurst S. Production of hydrogen by the steam-iron method. *J Am Oil Chem Soc*. 1939;16(2):29–36.
5. Anheden M, Svedberg G. Exergy analysis of chemical-looping combustion systems. *Energ Convers Manage*. 1998;39(16–18):1967–1980.
6. Dewulf J, Van Langenhove H, Muys B, Bruers S, Bakshi BR, Grubb GF, Paulus DD, Sciubba E. Exergy: Its potential and limitations in environmental science and technology. *Environ Sci Technol*. 2008; 42(7):2221–2232.
7. Ishida M, Zheng D, Akehata T. Evaluation of a chemical-looping-combustion power-generation system by graphic exergy analysis. *Energy*. 1987;2(2):147–154.
8. Jin HG, Ishida M. A new type of coal gas fueled chemical-looping combustion. *Fuel*. 2004;83(17–18):2411–2417.
9. Johansson M, Mattisson T, Lyngfelt A. Use of $NiO/NiAl_2O_4$ particles in a 10 kW chemical-looping combustor. *Ind Eng Chem Res*. 2006;45(17):5911–5919.
10. Gupta P, Velazquez-Vargas LG, Fan L.-S. Syngas redox (SGR) process to produce hydrogen from coal derived syngas. *Energy Fuel*. 2007;21(5):2900–2908.
11. Fan L.-S., Iyer M. Coal cleans up its act. *Chem Eng*. 2006:36–38.
12. Fan L.-S., Li F. Clean coal. *Phys World*. 2007;20(7):37–41.
13. Leion H, Mattisson T, Lyngfelt A. The use of petroleum coke as fuel in chemical-looping combustion. *Fuel*. 2007;86(12–13):1947–1958.
14. Lyngfelt A, Johansson M, Mattisson T. Chemical looping combustion - status of Development. The 9th International Conference on Circulating Fluidized Beds; 2008; Hamburg, Germany.
15. Fan, L.-S., Li F, Ramkumar S. Utilization of chemical looping strategy in coal gasification processes. *Particuology*. 2008;6(3):131–142.

16. Johansson E, Mattisson T, Lyngfelt A, Thunman H. A 300 W laboratory reactor system for chemical-looping combustion with particle circulation. *Fuel*. 2006;85(10–11):1428–1438.
17. Johansson E, Mattisson T, Lyngfelt A, Thunman H. Combustion of syngas and natural gas in a 300 w chemical-looping combustor. *Chem Eng Res Des*. 2006;84(A9):819–827.
18. Mattisson, T, Garcia-Labiano F, Kronberger B, Lyngfelt A, Adanez J, Hofbauer H. Chemical-looping combustion using syngas as fuel. *Int J Greenhouse Gas Control*. 2007;1(2):158–169.
19. Ryu, HJ, Jin GT, Bae DH, Yi CK. Continuous Operation of a 50 kWth Chemical-Looping Combustor: Long-Term Operation with Ni- and Co- Based Oxygen Carrier Particles. http://lib.kier.re.kr/balpyo/clean5/13.pdf. Accessed July 4th, 2008.
20. Kolbitsch, P, Bohar-Nordenkampf J, Proll T, Hofbauer H. Design of a chemical looping combustor using a dual circulating fluidized bed (DCFB) reactor system. The 9th International Conference on Circulating Fluidized Beds; 2008; Hamburg, Germany.
21. Svoboda K, Siewiorek A, Baxter D, Rogut J, Pohorely M. Thermodynamic possibilities and constraints for pure hydrogen production by a nickel and cobalt-based chemical looping process at lower temperatures. *Energy Convers Manage*. 2008;49(2):221–231.
22. Svoboda K, Slowinski G, Rogut J, Baxter D. Thermodynamic possibilities and constraints for pure hydrogen production by iron based chemical looping process at lower temperatures. *Energy Convers Manage*. 2007;48(12):3063–3073.
23. Xiang W, Chen Y. Hydrogen and electricity from coal with carbon dioxide separation using chemical looping reactors. *Energy Fuel*. 2007;21(4):2272–2277.
24. Fan L.-S., Li F, Velazquez-Vargas LG, Ramkumar S. Chemical looping gasification. The 9th International Conference on Circulating Fluidized Beds; 2008; Hamburg, Germany.
25. Li F, Fan L.-S. Clean coal conversion processes - progress and challenges. *Energy Environ Sci*. 2008;1:248–267.
26. Thomas T, Fan L.-S., Gupta P, Velazquez-Vargas LG. Combustion Looping using Composite Oxygen Carriers. US Patent 11010648. 2004.
27. Velazquez-Vargas LG, Gupta P, Li F, Fan L.-S. Hydrogen production from syngas using metal oxide composite particles. AIChE Annual Technical Meeting, 2005; Cincinnati, OH.
28. Velazquez-Vargas LG, Gupta P, Li F, Fan L.-S. Hydrogen production from coal derived syngas using novel metal oxide particles. International Pittsburgh Coal Conference; 2006; Pittsburgh, PA.
29. Elliott JF, Ralph RM, Stephenson RL. *Direct Reduced Iron: Technology and Economics of Production and Use*. Warrendale, PA: Iron & Steel Society of AIME; 1980.
30. Alcock CB. *Principles of Pyrometallurgy*. New York: Academic Press, Inc.; 1976.
31. Gaskell DR. *Introduction to Metallurgical Thermodynamics*. 2nd ed. New York: McGraw-Hill; 1981.
32. Gupta P, Velazquez-Vargas LG, Valentine C, Fan L.-S.. Moving bed reactor setup to study complex gas-solid reactions. *Rev Sci Instrum*. 2007;78(8):058106–1–085106–7.
33. AspenTech. *Aspen Physical Property System: Physical Property Methods and Models*. ASPEN Tech, Inc.; 2006.
34. Perry RH, Green DW. *Perry's Chemical Engineers' Handbook*. 8th ed. New York: McGraw-Hill; 2008.
35. Barin I. *Thermochemical Data of Pure Substances*. New York: Wiley-VCH; 1989.
36. Chase MW. *NIST-JANAF Thermochemical Tables*. 4th ed. Washington, DC: American Chemical Society; 1998.
37. Knacke O, Kubaschewski O, Hesselmann K. *Thermochemical Properties of Inorganic Substances*. 2nd ed. Berlin; New York: Springer-Verlag; 1991;129:2412.
38. Li F, Kim HR, Sridhar D, Wang F, Zeng L, Chen J, Fan L.-S. Syngas chemical looping gasification process: oxygen carrier particle selection and performance. *Energy Fuel*. 2008;23(8):4182–4189.
39. Wu S, Uddin MA, Sasaoka E. Effect of pore size distribution of calcium oxide high-temperature desulfurization sorbent on its sulfurization and consecutive oxidative decomposition. *Energy Fuel*. 2005;19(3):864–868.
40. Cachu S, Gunter WD. Acid gas injection in the Alberta Basin, Canada: a CO_2 storage experience. *Geo Soc S P*. 2004;233:225–234.

Manuscript received Mar. 24, 2009, and revision received Sept. 8, 2009.